The focusing performance with a horizontal time-reversal array at different depths in shallow water*

Zhang Tong-Wei(张同伟)†, Yang Kun-De(杨坤德), and Ma Yuan-Liang(马远良)

College of Marine, Northwestern Polytechnical University, Xi'an 710072, *China*

(Received 6 April 2010; revised manuscript received 29 June 2010)

The performance of time-reversal focusing with a horizontal line array at different depths is investigated by normal mode modeling and computer simulation. It is observed that the focusing performance of a bottom-mounted horizontal time-reversal array is much better than that of a horizontal time-reversal array at other depths in shallow water. The normal mode modeling is used to explain this result. The absolute values of the modes at different depths are compared. It is shown that the number of modes whose absolute values close to zero is smaller at the bottom than that at other depths. It means that the horizontal time-reversal array deployed at the bottom can sample more modes，obtain more information of the probe source and achieve better focusing performance. The numerical simulations of time-reversal focusing performance under various conditions, such as different sound speed profiles, and different bottom parameters, lead to similar results.

Keywords: time-reversal, horizontal line array, array depth

PACC: 4330, 9210V

1. Introduction

Most experiments of the time-reversal mirror[1−6] have been performed using a vertical line array which is a logical place to start in analytical and computational studies. Typically for a fixed location experiment, the vertical line array can be deployed from an anchored vessel and vertically aligned by a weight, or moored from the ocean floor and suspended by a float. However, the deployment of the vertical line array limits its flexibility and application.[7]

Practical implementation of the time reversal technology in the ocean may require use of horizontal line arrays (HLAs) that are bottom-mounted or towed. Acoustic time reversal and matched-field processing are somewhat conceptually similar but differ in their intent and requisite environment information. The utilization of horizontal line arrays to conduct acoustic time reversal is new, but much is already known in matched-field processing.[8−11] When dealing with time-reversal processing with an HLA, some methods can be borrowed from matched-field processing. Bogart and Yang[8] investigated and compared the matched-field processing performance between several bottom-mounted HLAs with different apertures and a full water column vertical line array in a simulated shallow water environment. Tantum and Nolte[12] proposed the general guidelines for matched-field processing array design especially for HLAs utilizing a normal mode propagation model. Dungan and Dowling[13] studied the orientation effects on linear time-reversal array retrofocusing in shallow water.

Recent studies only concerned with an HLA located at a special depth, and discussed the effects of the number of sensors and array length. However, array depth is another important factor that affects the spatial sampling capability of an HLA. In this paper, we compare the focusing performance with a horizontal time-reversal array (TRA) at different depths in shallow water. According to the normal mode theory,[14−17] the mode shape is a function of water depth and the m-th mode has m zeroes. Due to the depth dependence of the mode shape functions, when the number of sensors and array length meet the array design requirements,[12] the focusing performance achieved by a horizontal TRA depends on the depth

*Project supported by the National Natural Science Foundation of China (Grant No. 10774119), the Program for New Century Excellent Talents in University (Grant No. NCET-08-0455), the Natural Science Foundation of Shaanxi Province of China (Grant No. SJ08F07), the Foundation of National Laboratory of Acoustics, and the Northwestern Polytechnical University （NPU）Foundation for Fundamental Research.

†Corresponding author. E-mail: walternwpu@gmail.com

© 2010 Chinese Physics Society and IOP Publishing Ltd

at which the array is located.

The remainder of this article is organized into four sections. In the next section the formulation of acoustic time-reversal is reviewed and the performance evaluation metrics for time-reversal focusing are defined. In Section 3, the acoustic environment for the simulation study is described, and the simulation results are presented and explained. The numerical simulations under various conditions are given in Section 4. The similar results are obtained. Section 5 is a summary.

2. Theoretical background

2.1. Acoustic propagation model

For a unit harmonic point source of angular frequency ω located at $\boldsymbol{r}_0 = (0, z_\mathrm{s})$, the pressure field $p(\boldsymbol{r})$ at $\boldsymbol{r} = (r, z)$ is determined from Helmholtz equation[15]:

$$\nabla^2 p(r,z) + k^2(r,z)p(r,z) = -4\pi\delta(r)\delta(z - z_\mathrm{s}),$$
$$k(r,z) = \omega/c(r,z), \tag{1}$$

where z is taken positive in the downward direction. Normal mode theory expresses the acoustic field in terms of a normal mode expansion and then solves it for the eigenfunctions and eigenvalues which are solutions of the Helmholtz equation and satisfy the boundary conditions. The total acoustic pressure field is the weighted sum of the contributions of each mode. In cylindrical coordinates, equation (1) has a far-field solution for pressure which neglects the continuous spectrum of modes:

$$p(r,z) = \frac{\mathrm{i}\mathrm{e}^{-\mathrm{i}\pi/4}}{\rho(z_\mathrm{s})\sqrt{8\pi r}} \sum_{m=1}^{M} \Phi_m(z_\mathrm{s})\Phi_m(z)\frac{\mathrm{e}^{\mathrm{i}k_{rm}r}}{\sqrt{k_{rm}}}, \tag{2}$$

where the eigenfunction $\Phi_m(z)$ describes the shape of the m-th mode, and the eigenvalue k_{rm} is its associated horizontal propagation constant. The mode functions satisfy the orthonormality condition and form a complete set, allowing the total pressure field to be expressed as a sum of the modes as Eq. (2).

2.2. Acoustic time reversal

The theory of acoustic time reversal has already been presented.[1,2,13] The sketch map of time-reversal focusing with a horizontal TRA is shown in Fig. 1. The probe source (PS) is used to transmit the original signal. The horizontal TRA is the source-receiver array used to receive the PS transmitted signal, keep it in memory and send it back into the medium in the reversed direction of time. The VRA is the vertical receive array used to receive the time reversal field excited by the horizontal TRA and examine whether the sound focuses at the PS location.

The phase conjugation field at the field location (r, z) in frequency domain is written as[1,2]

$$P_\mathrm{pc}(r,z) = \sum_{n=1}^{N} p(r; z, z_n)p^*(R_n; z_n, z_\mathrm{s}), \tag{3}$$

where $p(R_n; z_n, z_\mathrm{s})$ represents the received field at the n-th receiver element of the TRA. R_n is the distance from the PS to the n-th receiver element, and z_n is the element depth. Likewise, $p(r; z, z_n)$ represents the field propagated from the n-th receiver element to the arbitrary receiver location (r, z). N is the number of TRA elements. Superscript $(*)$ denotes complex conjugate.

The imaginary part of the eigenfunction Φ_m is much less than its real part so $\Phi_m \simeq \Phi_m^*$ is often satisfied. The imaginary component of the horizontal wavenumber k_{rm} corresponds to attenuation. The greater the magnitude of the imaginary component, the more quickly the mode is attenuated. This implies that at a far distance from the source, the mode with a biggish imaginary component of horizontal wavenumber will have little contribution to the acoustic pressure field. Furthermore, the imaginary component of the horizontal wavenumber is much less than its real component in 3–4 orders of magnitude, so we have $k_{rm} \simeq k_{rm}^*$.

For a horizontal TRA uniformly spaced at d, all its elements are at the same depth z_a. The combination of Eqs. (2) and (3) yields:

$$P_\mathrm{Hpc}(r,z) = \sum_{n=1}^{N}\sum_{p=1}^{M}\sum_{m=1}^{M} \frac{\Phi_p(z)\Phi_p(z_a)\Phi_m(z_a)\Phi_m(z_\mathrm{s})}{\rho(z_a)\rho(z_\mathrm{s})8\pi\sqrt{k_{rp}k_{rm}r_nR_n}}\mathrm{e}^{\mathrm{i}(k_{rp}r_n - k_{rm}R_n)}, \tag{4}$$

where $R_n = R + (n-1)d$, $r_n = r + (n-1)d$, and R is the range from the PS to the first element of the horizontal TRA. The mode orthonormality condition cannot be used to simplify Eq. (4). In fact, Bartlett matched-field

processor with an HLA meets the similar problem, Bogart and Yang[8] handled the problem by separating the processor into diagonal and off-diagonal terms. Following Dungan and Dowling,[13] equation (4) can be separated into diagonal ($m = p$) and off-diagonal ($m \neq p$) terms:

$$P_{\mathrm{Hpc}}(r,z) = [P_{\mathrm{Hpc}}(r,z)]_{m=p} + [P_{\mathrm{Hpc}}(r,z)]_{m\neq p}, \tag{5a}$$

$$[P_{\mathrm{Hpc}}(r,z)]_{m=p} = \sum_{n=1}^{N}\sum_{m=1}^{M} \frac{\Phi_m(z)\Phi_m^2(z_a)\Phi_m(z_{\mathrm{s}})}{\rho(z_a)\rho(z_{\mathrm{s}})8\pi k_{rm}\sqrt{r_n R_n}} \mathrm{e}^{\mathrm{i}k_{rm}(r_n - R_n)}, \tag{5b}$$

$$[P_{\mathrm{Hpc}}(r,z)]_{m\neq p} = \sum_{n=1}^{N}\sum_{p\neq m}^{M}\sum_{m=1}^{M} \frac{\Phi_p(z)\Phi_p(z_a)\Phi_m(z_a)\Phi_m(z_{\mathrm{s}})}{\rho(z_a)\rho(z_{\mathrm{s}})8\pi\sqrt{k_{rp}k_{rm}r_n R_n}} \mathrm{e}^{\mathrm{i}(k_{rp}r_n - k_{rm}R_n)}. \tag{5c}$$

For the field at the PS, $r = R$, equations (5b) and (5c) can be made further simplification:

$$[P_{\mathrm{Hpc}}(R,z)]_{m=p} = \sum_{n=1}^{N}\sum_{m=1}^{M} \frac{\Phi_m(z)\Phi_m^2(z_a)\Phi_m(z_{\mathrm{s}})}{\rho(z_a)\rho(z_{\mathrm{s}})8\pi k_{rm}(R + (n-1)d)}, \tag{6a}$$

$$[P_{\mathrm{Hpc}}(R,z)]_{m\neq p} = \sum_{n=1}^{N}\sum_{p\neq m}^{M}\sum_{m=1}^{M} \frac{\Phi_p(z)\Phi_p(z_a)\Phi_m(z_a)\Phi_m(z_{\mathrm{s}})}{\rho(z_a)\rho(z_{\mathrm{s}})8\pi(R + (n-1)d)\sqrt{k_{rp}k_{rm}}} \mathrm{e}^{\mathrm{i}(k_{rp} - k_{rm})(R + (n-1)d)}. \tag{6b}$$

The complex phase factor in Eq. (6b) will distribute real and imaginary parts over both positive and negative values, so the off-diagonal terms will tend to cancel with each other as long as the array satisfies the minimum length requirement and contains enough elements. There is an additional factor $\Phi_m^2(z_a)$ in each term of Eq. (6a). This additional factor will modulate the mode amplitudes. Such mode-amplitude modulation can be important. If the array depth coincides with a zero crossing in a mode amplitude function, then the particular mode does not contribute to the received pressure field along the array, and the information it contains about the PS is lost. Because the additional factor is a function of horizontal TRA depth, the array depth will directly affect its mode sampling capability, and then the focusing performance with a horizontal TRA depends on its depth.

2.3. Performance metric

In order to evaluate the time-reversal focusing performance, the correct focusing index (CFI) and the focusing characteristic index (FCI) are used. The CFI is defined as $10\log(N+1)$, where N is the grid number where the ambiguity function level is greater than those at the PS location and its neighborhood. When N equals zero, it means that the peak appears at the PS location. So the value of CFI equals 0 dB for correct focusing at the PS location and *vice versa*. FCI is defined as $10\log(M+1)$, where M the grid number, and the ambiguity function level (the greatest output power normalized to be 0 dB) is greater than -3 dB. That means the output power values at those grids are greater than the half of the greatest output power. The FCI is used to indicate the output interference noise level on the ambiguity surface.

3. Numerical experiments

3.1. Ocean environment model

The ocean environment used in this study is shown in Fig. 1. It is an ideal range-independent shallow water sound channel. The water depth is 100 m. The sound speed in water is modeled as a typical summer profile. The ocean surface is treated as a flat pressure-release surface. A sediment layer of

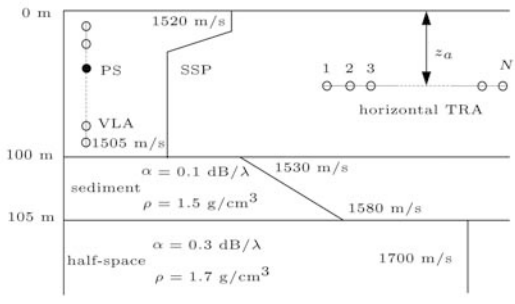


Fig. 1. Computational range-independent shallow water sound channel with geometric and environmental parameters. The horizontal TRA locates at a specific depth with its first element nearest to the PS. The PS is fixed at end-fire to the horizontal TRA.

5-m thick can be included between the water and the bottom. The bottom and sediment are described in the KRAKEN model[18] by their sound speeds, densities, and attenuations.

Assuming that the whole environment is not changed with time[19] and the ambient noise is ignored. The source range is defined as the horizontal distance from the PS to the first element of the horizontal TRA. The PS is fixed at the endfire to the horizontal TRA. If the PS is at some other bearings, then the array is effectively shorter and the elements are more closely spaced.

The mode shape functions Φ_m and the corresponding horizontal wavenumber k_{rm} are calculated with the KRAKEN normal mode model. For a 500-Hz source, the ocean environment of Fig. 1 supports 32 modes. The array designs should be based on $\pi/k_{\rm M} < d < 2\pi/(k_1 - k_{\rm M})$ and $\min(k_{m-1} - k_m)L \geq 1$. In fact, the minimum number of elements $N_{\min}$ can be estimated from the largest d and the smallest L[13]:

$$N_{\min} \approx 1 + \frac{k_1 - k_{\rm M}}{2\pi \times \min(k_{m-1} - k_m)}. \qquad (7)$$

For the waveguide of Fig. 1, $k_1 = 2.0871$ m^{-1} and $k_{\rm M} = k_{32} = 1.8518$ m^{-1}, so this estimate yields $N_{\min} \approx 35$, $L = (N-1) \times d = (35-1) \times [2\pi/(k_1 - k_{\rm M})] \approx 910$ m, and $d = 2\pi/(k_1 - k_{\rm M}) \approx 27$ m. Thus the horizontal TRA consists of 35 hydrophones uniformly spaced every 27 m in a range over an aperture length $L_{\rm a}$ equal to 910 m. The range between the PS and the first element of horizontal TRA is 12 km.

3.2. The focusing performance with a horizontal TRA at different depths

The PS locates under the thermocline at a depth of 40 m. The depth of the horizontal TRA increases from 1 m to 100 m with an increment of 1 m. The ambiguity surfaces are computed from 1 m to 100 m in depth, at 1-m interval, and from 10.5 km to 13.5 km in range, at 10-m interval. The focusing performance curves with the horizontal TRA at different depths are plotted in Fig. 2. Figure 2(a) shows that the correct focusing index (CFI) is affected significantly by the array depth. The horizontal TRA can focus the sound back to the PS location correctly when it locates at some special depths, such as near the bottom. As shown in Fig. 2(b), the FCI is much better at the bottom (0 dB) than other depths (> 8 dB). Compared with other depths, the horizontal TRA mounted at the bottom can achieve the best focusing performance.

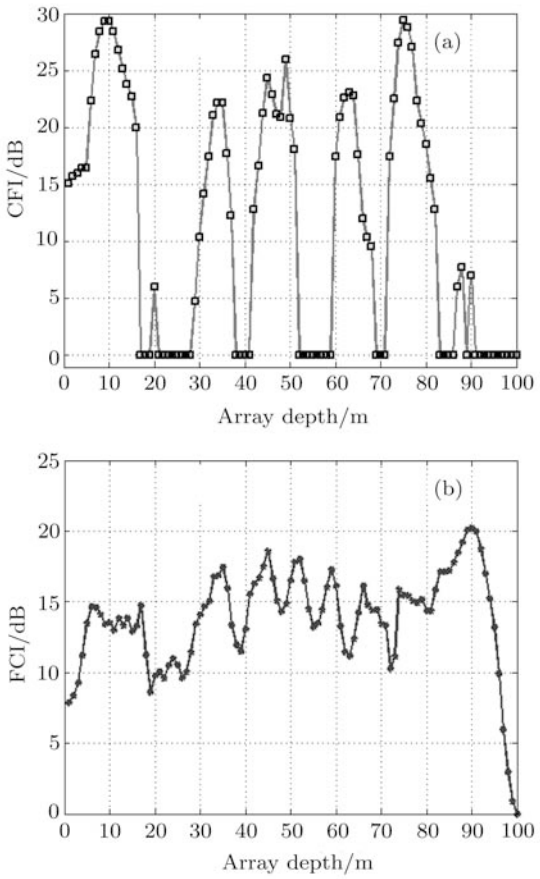


Fig. 2. The focusing performance curves for a PS located at 40-m depth with a horizontal TRA at different depths. (a) The correct focusing index which indicates whether a horizontal TRA located at a specific depth can make a correct focusing. (b) The focusing characteristic index (FCI) describes the output interference noise level on the ambiguity surface.

In order to have a good understanding of the CFI and FCI shown in Fig. 2, the ambiguity surfaces for a horizontal TRA locate at three different depths (49 m, 79 m, and 100 m) are shown in Fig. 3. Figures 3(a) and 3(b) show that the peaks do not appear at the PS position in both cases. There are many strong sidelobes, and their corresponding FCIs are 15 dB and 14 dB, respectively. When the horizontal TRA locates at 100 m, figure 3(c) shows that the focusing peak appears at the PS position correctly and the strong sidelobes are suppressed successfully.

The modes calculated by the KRAKEN are analysed to explain this result. For a 500-Hz source, the first 20 modes supported by this ocean environment are illustrated in Fig. 4. Each mode is normalized. It is obtained that the mode amplitudes change rapidly

with depth and the amplitudes of some modes (2, 9, 10, 13, 16, and 18th) are nearly close to zero at a certain depth (65 m). This means that a horizontal

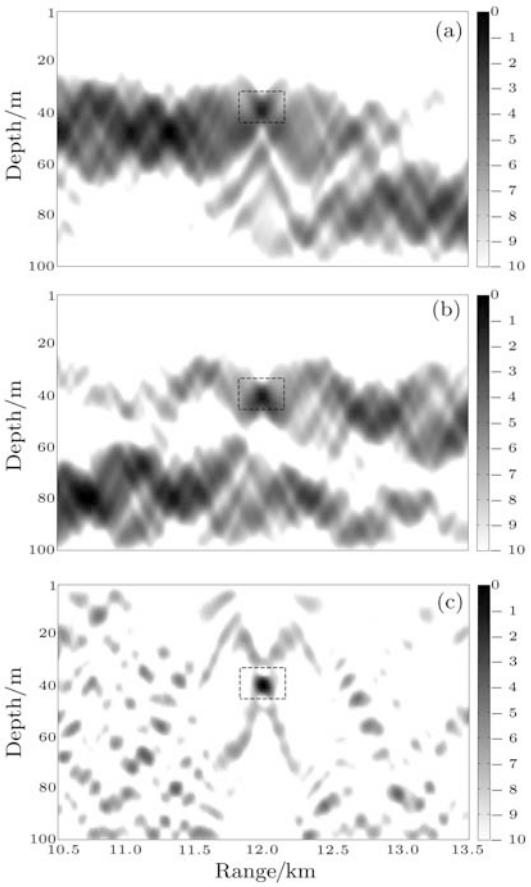


Fig. 3. The ambiguity surfaces for a horizontal TRA locate at three different depths: (a) 49 m, (b) 79 m, and (c) 100 m.

TRA located at such a depth will lack the contributions from those modes, and the information about the PS contained in these modes will be lost.

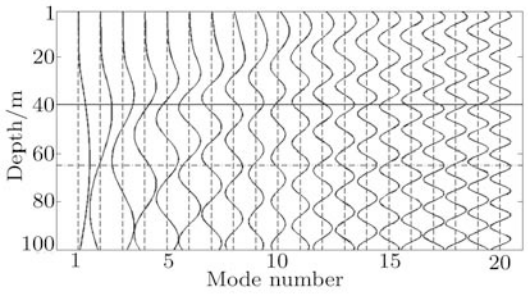


Fig. 4. The first 20 modes propagating in the sound channel at 500 Hz. Each mode is normalized.

The absolute values of the modes at different depths are compared. Figure 5 shows the numbers of modes (NM) whose absolute values are less than half of its maximum amplitude at different depths. Notice that NM is smaller at the bottom than other depths. It implies that there are more modes contributing to the acoustic pressure field at the bottom than other depths. And then the horizontal TRA located at the bottom can sample more modes, obtain more information about the PS and achieve better time-reversal focusing performance.

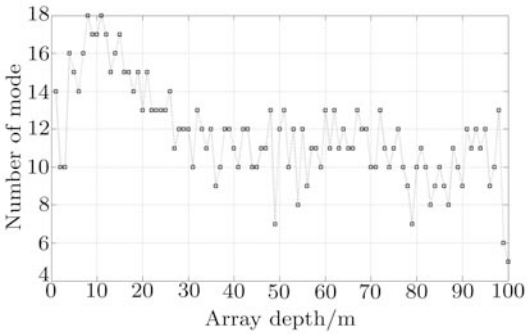


Fig. 5. The number of modes whose absolute value less than half of the maximum amplitude value at different depths for a 500-Hz source.

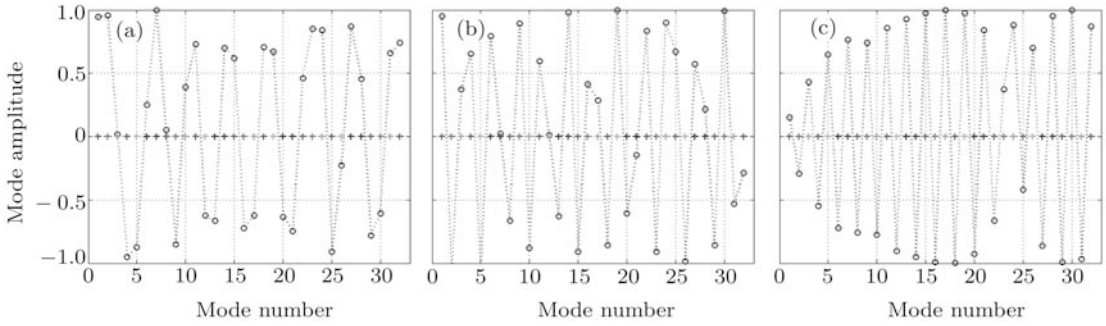


Fig. 6. Normalized mode amplitudes calculated by the KRAKEN at three depths for a 500-Hz source: (a) 49 m, (b) 79 m, and (c) 100 m.

In addition, NMs are also small at 49 m and 79 m, but the focusing performance with a horizontal TRA deployed at these two depths are very poor (see Figs. 2 and 3). Figure 6 shows the mode amplitudes at 49-, 79- and 100-m depths. There are two modes whose values are nearly close to zero at 49 m and 79 m, respectively, and the information about the PS contained in those modes is nearly lost. However, for the case of the array located at the bottom, though there are 5 modes whose absolute values are less than half of its maximum amplitude, the mode values of these 5 modes are not close to zero, and the smallest one is the first mode whose mode value is 0.2. Therefore, the mode sampling ability of the horizontal TRA is much better at the bottom than that at 49 m and 79 m.

4. Environmental effects on the focusing performance with a horizontal TRA

The above simulation and discussion show that the focusing performance of a bottom-mounted horizontal TRA is much better than that of a horizontal TRA at other depths in shallow water as specified in Fig. 1. A physical interpretation of this result is given through the normal mode modeling. From the point of view of the theory and practice of acoustic sensing, there are a variety of factors that affect the propagation of sound in shallow water waveguide. The most important ones among them are the shape of the sound-speed profile (SSP) and the geoacoustic properties of the bottom. Other parameters which include roughnesses of the bottom, surface disturbance, random inhomogeneities in the water layer, sea currents, etc. alter the sound field. In comparison with the first two factors, the role of the latter is on the whole less marked for lower frequencies.

The numerical simulations of focusing performance under various conditions, such as different SSPs, and different bottom parameters, are presented in this section. The environmental and system parameters used in this section are the same as those previous used unless specially described. It should be noted that the FCI cannot be compared with each other when changing the environment parameters because it is normalized.

4.1. SSP effect

Another two SSPs are chosen to analyse the SSP effect on the focusing performance with a horizontal TRA at different depths. One is modeled as a downward refracting linear profile (1520–1505 m/s). The other is isovelocity at 1500 m/s. Figure 7 shows the focusing performance curves with a horizontal TRA at different depths. In an isovelocity sound channel, both the surface- and bottom-mounted horizontal TRA can achieve high-quality focusing performance. The focusing performance achieved with a bottom-mounted horizontal TRA is the best when the SSP is a downward refracting linear profile. It should be noticed that when a horizontal TRA locates near the surface, high-quality focusing can still be achieved.

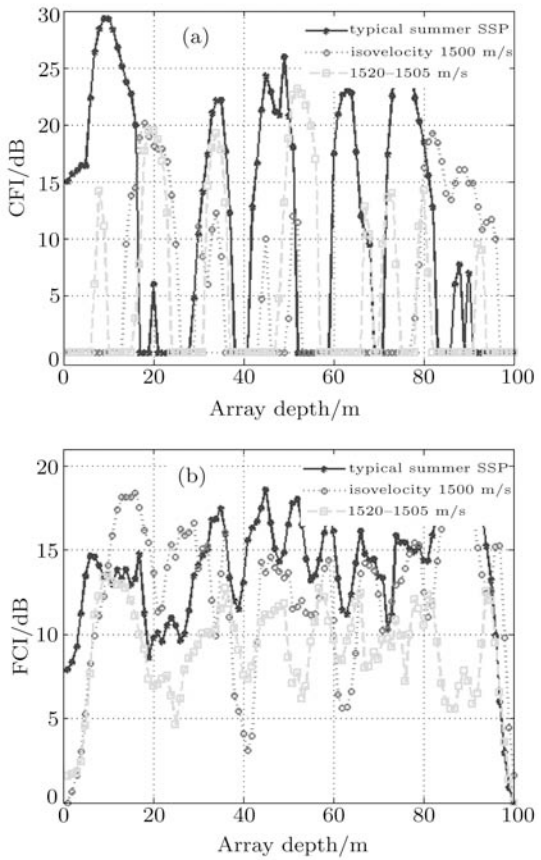


Fig. 7. The focusing performance curves affected by different SSPs. (a) The correct focusing index. (b) The focusing characteristic index.

4.2. Sediment sound speed effect

Figure 8 shows the focusing performance curves with a horizontal TRA at different depths for different sediment sound speeds. Notice that for all these three sediment sound speeds, the focusing per-

formance achieved with a bottom-mounted horizontal TRA is the best. The larger the sediment sound speed is, the bigger the number of depths where a horizontal TRA can focus the sound back to its original is. As the sediment sound speed increases, the reflection coefficient becomes larger. It means that more energy will be reflected back to the water from the bottom interface. So the horizontal TRA can obtain more information and achieve correct focusing at more depths with a larger sediment sound speed.

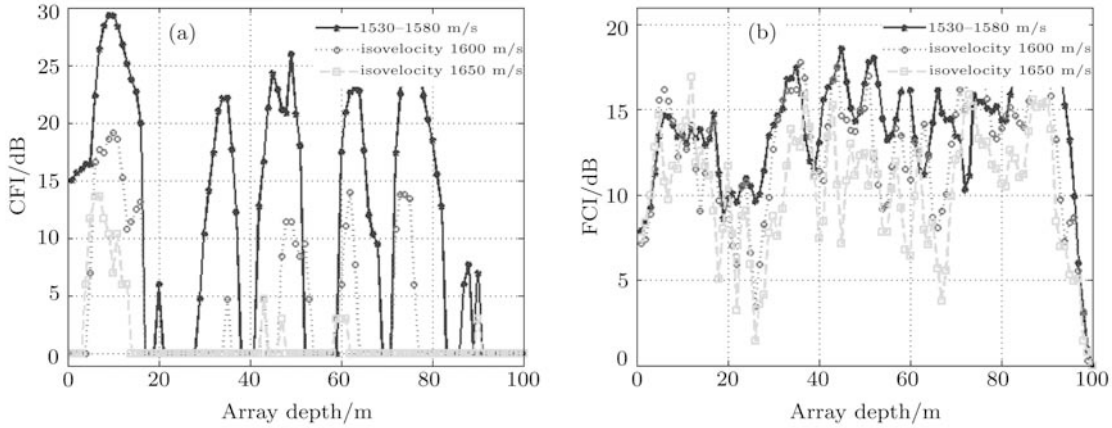


Fig. 8. The focusing performance curves affected by different sediment sound speeds. (a) The correct focusing index. (b) The focusing characteristic index.

4.3. Sediment thickness effect

Figure 9 shows the focusing performance curves with a horizontal TRA at different depths for three different sediment thicknesses. It is observed that for different sediment thicknesses the focusing performance achieved with a bottom-mounted horizontal TRA is the best. Figure 9(a) also shows that as the sediment thickness increases, the number of depths where a horizontal TRA can make correct focusing becomes smaller. This is because there will be more energy transmitted into the sediment at a thicker sediment.

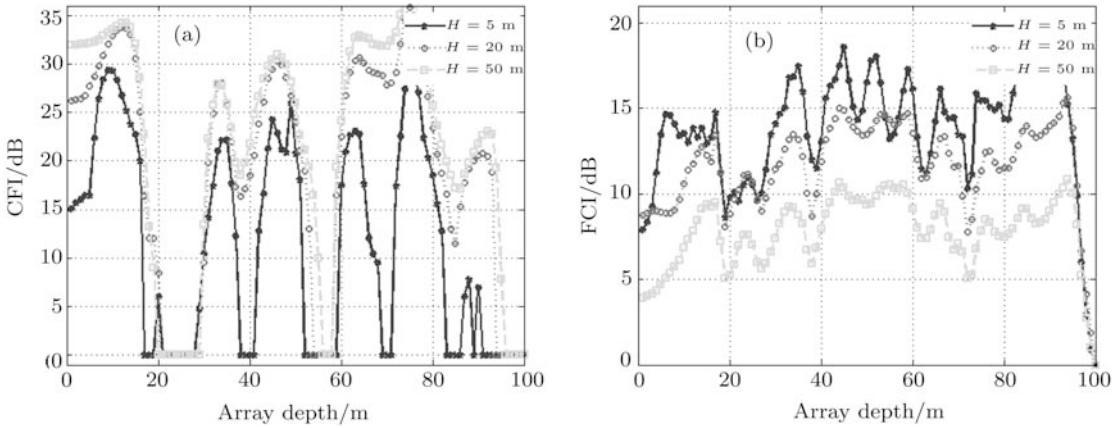


Fig. 9. The focusing performance curves affected by different sediment thicknesses. (a) The correct focusing index. (b) The focusing characteristic index.

4.4. Sediment attenuation effect

Figure 10 shows the focusing performance curves with a horizontal TRA at different depths for three different sediment attenuations. For different sediment attenuations, the focusing performance achieved with a

bottom-mounted horizontal TRA is the best. Figure 10(a) also shows that as the sediment attenuation increases, the number of depths where a horizontal TRA can make correct focusing becomes smaller. For example, when $\alpha = 0.3$ dB/λ, there are only two areas (one is the middle of the thermocline, the other is near the bottom) where a horizontal TRA can make correct focusing. This is because there will be more energy attenuated at a sediment with larger attenuation.

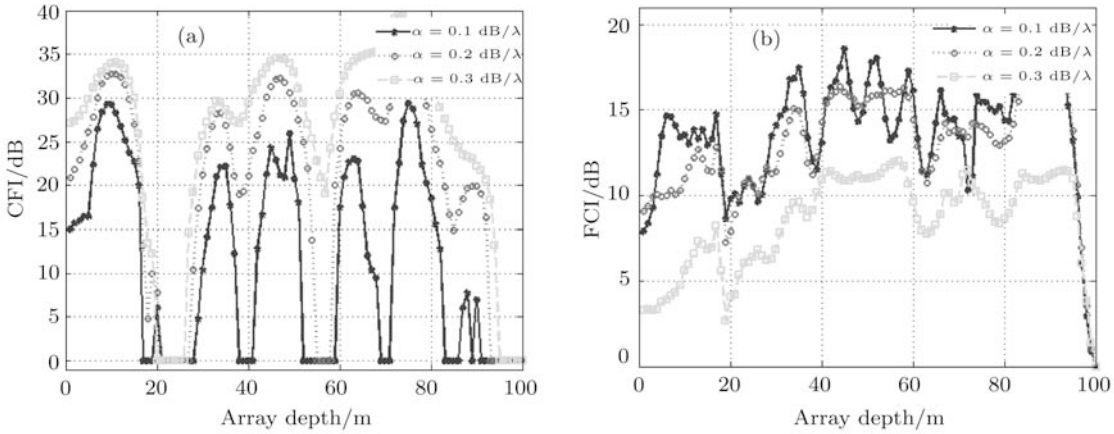


Fig. 10. The focusing performance curves affected by different sediment attenuations. (a) The correct focusing index. (b) The focusing characteristic index.

5. Summary

This paper has analysed the focusing performance with a horizontal TRA at different depths in shallow water. It is observed that a bottom-mounted horizontal TRA can not only have correct focusing, but also suppress strong sidelobes, while a horizontal TRA at other depths cannot. The normal mode modeling is used to give a physical explanation to this result. The essential reason is that the real ocean bottom is neither perfectly rigid nor perfectly soft. Some sound energy will transmit into the bottom from water. It means that each mode has a tail at the bottom, and the mode amplitude is bigger than zero at the bottom. However, there are always some modes whose amplitudes close to zero at other depths. When the number of sensors and array length meet the array design requirements, the bottom-mounted horizontal TRA can obtain more information about the PS and achieve better focusing performance than other depths.

The numerical simulations of focusing performance are presented under various conditions, such as different sound speed profiles, and different bottom parameters. It is confirmed that the results are similar.

It is hoped that the results in this paper should be verified experimentally in the future.

References

[1] Jackson D R and Dowling D R 1991 *J. Acoust. Soc. Am.* **89** 171

[2] Kuperman W A, Hodgkiss W S, Song H C, Akal T, Ferla C and Jackson D R 1998 *J. Acoust. Soc. Am.* **103** 25

[3] Song H C, Kuperman W A and Hodgkiss W S 1998 *J. Acoust. Soc. Am.* **103** 3234

[4] Hodgkiss W S, Song H C, Kuperman W A, Akal T, Ferla C and Jackson D R 1999 *J. Acoust. Soc. Am.* **105** 1597

[5] Fink M, Cassereau D, Derode A, Prada C, Roux P, Mickael Tanter, Thomas J L and Wu F 2000 *Rep. Prog. Phys.* **63** 1933

[6] Kim J S, Song H C and Kuperman W A 2001 *J. Acoust. Soc. Am.* **109** 1817

[7] Li X, Yang K, Zhang T and Qiu H 2009 *Acta Phys. Sin.* **58** 7741 (in Chinese)

[8] Bogart C W and Yang T C 1994 *J. Acoust. Soc. Am.* **96** 1677

[9] Yang T C and Bogart C W 1994 *J. Acoust. Soc. Am.* **95** 3149

[10] Siderius M, Nielsen P L and Gerstoft P 2003 *IEEE J. Ocean. Eng.* **28** 424

[11] Fialkowski L T, Yang T C, Yoo K, Kim E and Dacol D K 2006 *J. Acoust. Soc. Am.* **120** 231

[12] Tantum S L and Nolte L W 2000 *J. Acoust. Soc. Am.* **107** 2101

[13] Dungan M R and Dowling D R 2002 *J. Acoust. Soc. Am.* **112** 1842

[14] Wang N and Liu J 2002 *Chin. Phys.* **11** 456

[15] Jensen F B, Kuperman W A, Porter M B and Schmidt H 1994 *Computational Ocean Acoustics* (New York: AIP Press) p. 257

[16] Zhang R H and Li F H 1999 *Sci. Chin.* Ser. A **42** 739 (in Chinese)

[17] Yu Y, Hui J, Zhao A, Sun G and Teng C 2008 *Acta Phys. Sin.* **57** 5742 (in Chinese)

[18] Porter M B 1991 *The KRAKEN Normal Mode Program*, Technical Report, SACLANT Undersea Research Center

[19] Song J 2006 *Chin. Phys.* **15** 2796